Engineering quantum correlations for $m \times n$ spatially encoded two-photons states

P. Machado, A. A. Matoso, M. R. Barros, L. Neves, and S. Pádua
Departamento de Física, Universidade Federal de Minas Gerais, 31270-901 Belo Horizonte, Minas Gerais, Brazil

(Received 14 December 2018; published 28 June 2019)

Discretizing transverse linear momentum of photon pairs, generated by spontaneous parametric down conversion (SPDC), is one of the simplest methods for producing bipartite entangled states in high dimensions. So far, it has been employed only to prepare states in dimensions $m \times m$. In this work, we study the generalization for engineering entangled states in dimensions $m \times n$. Our approach relies on the manipulation of the pump beam transverse profile and the phase-matching function of the SPDC process to prepare, behind an m- and n-slit aperture, different $m \times n$ spatial entangled states. We demonstrate the technique experimentally for some 2×3 states. Compared to previous approaches in producing $2 \times n$ photonic entanglement, which require either more than two photons or hybrid entanglement, our scheme is less demanding and simpler since we employ only two photons and a single degree of freedom to encode the states.

DOI: 10.1103/PhysRevA.99.063839

I. INTRODUCTION

Over the past 30 years spontaneous parametric down conversion (SPDC) has been the main process used to obtain entangled photonic states. The inherent characteristics of the phenomenon allows the construction of states correlated in many degrees of freedom, providing an useful resource for experimental studies in quantum communications, quantum information, and in fundamentals of quantum physics [1–3].

When preparing spatially encoded states using SPDC, two aspects have to be taken into account, namely, the crystal characteristics and the pump beam transverse profile [4,5]. The influence of the first was already extensively studied in [6–10]. The second aspect, with the intention of engineering entangled states and controlling twin photons correlations by regulating the pump beam shape, has been done both manually and electronically, preparing photonic states encoded in continuous and discrete variables [11–15]. The possibility to govern the biphoton state by modifying the pump beam has been studied over the years and was recently explored in preparing two qudits states with dimension $m \times m$ in an angular momentum degree of freedom [16,17]. In their useful method two qudits states of equal dimensions ($d = 3$, 4, and 5) are prepared by using two spatial light modulators at the pump beam and twin photons paths without the need of spatial filtering and with the possibility of amplitude and phase control. Unlike these works, we study the possibilities of modifying the pump profile and the propagated phase-matching function to prepare bipartite quantum states in linear momentum degree of the photon pairs. In our work we are interested in preparing two qudits states in dimension $m \times n$ ($m \neq n$), where m and n define the possible photons' paths after they cross different slit sets. The controlling of pump beam has been found useful in applications as for example to maintain the spatial correlations when the photons propagate in a turbulent media [18,19].

Bipartite entangled states have been prepared by using different degrees of freedom of the photons as polarization [20], angular momentum [14,21–23], frequency [24], and transverse path [25]. Concerning this last one, different methods for engineering spatial bipartite states can be found in the literature. In all of them, multiple slits are placed transversally at photons paths discretizing their linear momentum. However, until now, only the preparation of $m \times m$ spatial states has been studied [26]. Polarization degree of freedom has been already explored in preparation of 2×3 states by means of a complex arrangement of four photons in [27], and in a simpler proposal to preparation of $2 \times n$ states, using hybrid entanglement, made in [28]. Therefore, to study new forms to encode these states in spatial variables is important to decrease experimental complexity and to increase the number of possible correlations that one can prepare experimentally.

In previous works, involving only spatial states, when photonic entangled states are generated in path variables, each photon was intercepted by apertures with the same number of slits. In this paper, we analyze the use of known methods in preparation of $m \times n$ states introducing some correlations that arise when a different number of apertures are placed at the paths of each of the twin photons. We show how to set a two-photons system needed for an experimental implementation of theoretical studies involving $m \times n$ quantum states.

The preparation of bipartite quantum states of dimension $m \times n$ ($m \neq n$) is, in different contexts, necessary for answering interesting fundamental questions. Khoury and Oxman studied the appearance of the fractional topological phase and its structure for two qudits systems of dimension $m \times n$ in general and for the particular qubit-qutrit system [29]. Ann and Jagger have demonstrated theoretically entanglement sudden death in a qubit-qutrit system where the systems are individually incoherent but may still have coherence and entanglement in the composite system [30]. Karpak and Gedik studied theoretically the time evolution of the classical and quantum correlations of qubit-qutrit systems in independent and common dephasing environments [31] and later extended for various decoherent channels. An analytical expression of quantum discord for a class of states in qubit-qutrit systems was derived and its dynamics was studied for various

 ©2019 American Physical Society

dissipative systems [32]. Increasing the dimension of only one part of the system is therefore essential in the experimental implementation of theoretical studies as fundamental tests in quantum mechanics [33–35], analysis of the dynamic of 2×3 quantum states [31,36,37], the measurement of topological phase of 2×3 quantum states [29], and quantum coarse-graining analyses [38]. In this work we aim to show that these states can be prepared exploring the linear momentum of twin photons generated by SPDC, and also discuss their behavior face to some interference measurements.

The paper is organized as follows. In the next section we present an overview about the photonic quantum states prepared on photon path variables, defined by multiple slits. In Sec. III we analyze the correlations that one can obtain when different state preparation methods are applied to 2×3 and 3×4 states. We also analyze, in Sec. IV, the interference patterns resulted from some 2×3 states and propose a method to study spatial correlations in these states by means of measurement in different bases (position momentum). Later, in Sec. V, we show that the relation between the conditional interference and entanglement in 2×3 photons states cannot be made directly. Finally, we conclude in Sec. VI.

II. OVERVIEW ABOUT SPATIAL STATES ENGINEERING BEHIND MULTIPLE-SLIT APERTURES

Spatial entanglement between photons generated by SPDC occurs due to the nonseparability of biphoton amplitude, which is a joint result of the spatial properties of the pump beam, transferred to the photon pair, and the phase-matching function (PMF). The photons generated in the SPDC process are usually named signal (s) and idler (i) photon [39]. Disregarding the polarization information and using the formalism developed in [5,40] to one spatial dimension and degenerated photons, we can write down the biphoton state at some transverse plane at z as

$$|\psi_z\rangle \propto \iint \Phi(x_s, x_i, z)|x_s\rangle|x_i\rangle dx_s dx_i, \tag{1}$$

where $|x_s\rangle|x_i\rangle$ is defined as

$$|x_s\rangle|x_i\rangle = \frac{1}{4\pi^2}\int dq_s e^{ix_s q_s}|q_s\rangle \int dq_i e^{ix_i q_i}|q_i\rangle, \tag{2}$$

and $|q_s\rangle$, $|q_i\rangle$ are the Fock states that represent photons with transverse momentum q_s and q_i.

The function $\Phi(x_s, x_i, z)$ is a product of two nonseparable functions in spatial variables $E[(x_i + x_s)/2]$ and $\xi(x_i - x_s)/2$, namely

$$\Phi(x_s, x_i, z) = E\left(\frac{x_i + x_s}{2}, z\right)\xi\left(\frac{x_i - x_s}{2}, z\right), \tag{3}$$

where $E((x_i + x_s)/2, z)$ is the pump beam transverse amplitude, written in terms of the twin variables, and $\xi((x_i - x_s)/2, z)$ is the PMF propagated to the plane at z which depends on crystal properties and on the difference of the photon spatial variables, and for which we do not consider the Gaussian approximation [9]. Although the Gaussian approximation for the PMF has been used for some authors [41–46] it has been shown by Gómez *et al.* that the spatial state of SPDC cannot be seen as a two-mode Gaussian entangled state even when it is pumped by a Gaussian pump beam and for a perfect phase matching condition [47]. In this work, we discuss the two-photons state in spatial variables by analyzing it in terms of both functions $E((x_i + x_s)/2, z)$ and $\xi((x_i - x_s)/2, z)$. In this scenario both functions cannot be factorized in a product of individual functions of x_i and x_s. When an aperture with D_α slits ($\alpha = i, s$) is placed in the path of each photon, the biphoton state immediately after the apertures is [48]

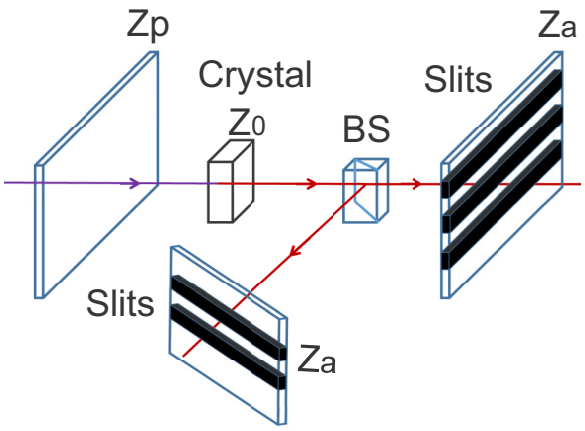

FIG. 1. Graphic layout of a general state preparation setup with the twin photons generated by SPDC collinearly and then separated by a beam splitter. The nonlinear crystal and the slits are positioned, respectively, in the planes at z_0 and z_a. z_p is the position of a plane before the crystal.

$$|\psi_f\rangle \propto \sum_{l_i=-\Lambda_i}^{\Lambda_i}\sum_{l_s=-\Lambda_s}^{\Lambda_s} \Phi_{\text{in}}(l_i d, l_s d, z_a)|l_i\rangle|l_s\rangle, \tag{4}$$

where z_a is the position of the apertures plane, $\Lambda_\alpha = (D_\alpha - 1)/2$, d is the distance between two slits, $\Phi_{\text{in}}(x_i, x_s, z_a)$ is the biphoton amplitude on the plane at z_a, and $|l_\alpha\rangle$ ($\alpha = i, s$) is the quantum state of a photon α which passes through slit l. The qudits dimensions, defined by D_α, are independent from each other, so one could diversify the number of slits in the multiple slit set for each photon of the pair aiming the construction of $m \times n$ states. So far, only $m \times m$ states have been explored. Regardless of the experimental setup, state preparation behind the multiple slits seeks the manipulation of the biphoton amplitude function at specific points, such that it controls the correlations between each pair of modes $|l_i\rangle|l_s\rangle$. The main issue in this work is how to manipulate biphoton amplitude to produce specific $m \times n$ photonic entangled path states. Here, we shall consider two approaches.

(i) Manipulating PMF: when an enlarged image of the crystal, positioned on a plane at z_0, is projected onto a plane at z_a (Fig. 1), the biphoton amplitude at the apertures is equal to the amplitude at the crystal exit, scaled by a magnification constant and multiplied by a phase factor. In this case, the pump transverse profile at z_a is wider than the PMF at this plane. Thus the transverse pump amplitude is approximately constant along the slits and the correlations are predominantly controlled by the PMF width at z_a [10].

(ii) Manipulating the pump beam transverse profile: if the image of some plane at z_p, before the crystal, is projected on

z_a (Fig. 1) in a setup where the thin crystal approximation is valid, the PMF is approximately constant along the slits. Then, controlling the pump shape at z_a (or z_p) is equivalent to controlling the correlations between the slits [14,25]. In the next section, we describe in detail the manipulation of both PMF and pump beam profile, and present possible correlations that one can achieve in $m \times n$ spatially encoded two-photons states.

III. ENGINEERING OF THE $m \times n$ TWO-PHOTONS SPATIAL CORRELATIONS

In face of Eq. (4) some questions arise. Are the number of correlations, obtained making photons cross different numbers of slits, limited somehow? How do these possible correlations look? Are there maximally entangled states amongst them? In this section, we aim to answer these questions discussing possibilities and limitations for the correlations that one can obtain by means of the methods mentioned in the last section. To illustrate the problem in a simple manner, we analyze the specific cases of dimensions 2×3 and 3×4. We study specific cases, for illustration, but analogous analyses can be done for any dimension.

A. Manipulating PMF

If an enlarged image of the crystal is projected on a plane at z_a, the state of Eq. (4) can be written as [39]

$$|\psi\rangle \propto \sum_{l_i=-\Lambda_i}^{\Lambda_i} \sum_{l_s=-\Lambda_s}^{\Lambda_s} e^{i\varphi(l_i^2+l_s^2)} \xi\left(\frac{(l_i-l_s)d}{2p}, z_0\right) \times E\left(\frac{(l_i+l_s)d}{2p}, z_0\right)|l_i\rangle|l_s\rangle, \tag{5}$$

where φ is a phase acquired along the propagation that depends of the setup characteristics, p is the magnification of the image, and z_0 is the position of the crystal plane. We can represent a $m \times n$ pure state by means of a coefficient matrix $M_{m\times n}$. For instance, considering 2×3 and 3×4 dimensions in the context of the manipulation of the PMF image we have

$$M^{(\mathrm{PMF})}_{2\times 3} = \begin{array}{c} \\ |-\frac{1}{2}\rangle \\ |\frac{1}{2}\rangle \end{array} \begin{array}{c} \begin{array}{ccc} |-1\rangle & |0\rangle & |1\rangle \end{array} \\ \begin{pmatrix} \xi_1 \times E_2 e^{i\varphi} & \xi_1 \times E_1 & \xi_2 \times E_1 e^{i\varphi} \\ \xi_2 \times E_1 e^{i\varphi} & \xi_1 \times E_1 & \xi_1 \times E_2 e^{i\varphi} \end{pmatrix} \end{array}, \tag{6}$$

and

$$M^{(\mathrm{PMF})}_{3\times 4} = \begin{array}{c} \\ |-1\rangle \\ |0\rangle \\ |1\rangle \end{array} \begin{array}{c} \begin{array}{cccc} |-\frac{3}{2}\rangle & |-\frac{1}{2}\rangle & |\frac{1}{2}\rangle & |\frac{3}{2}\rangle \end{array} \\ \begin{pmatrix} \xi_1 \times E_3 e^{3i\varphi} & \xi_1 \times E_2 e^{i\varphi} & \xi_2 \times E_1 e^{i\varphi} & \xi_3 \times E_1 e^{3i\varphi} \\ \xi_2 \times E_2 e^{2i\varphi} & \xi_1 \times E_1 & \xi_1 \times E_1 & \xi_2 \times E_2 e^{2i\varphi} \\ \xi_3 \times E_1 e^{3i\varphi} & \xi_2 \times E_1 e^{i\varphi} & \xi_1 \times E_2 e^{i\varphi} & \xi_1 \times E_3 e^{3i\varphi} \end{pmatrix} \end{array}, \tag{7}$$

where $\xi_1 = \xi(\frac{d}{4p}, z_0)$, $\xi_2 = \xi(\frac{3d}{4p}, z_0)$, $\xi_3 = \xi(\frac{5d}{4p}, z_0)$, $E_1 = E(\frac{d}{4p}, z_0)$, $E_2 = E(\frac{3d}{4p}, z_0)$, $E_3 = E(\frac{5d}{4p}, z_0)$, and the biphoton amplitude was assumed to be symmetrical.

As described previously, the correlations in Eqs. (6) and (7) are predominantly controlled by the coefficients ξ_j defined by the PMF image. For example, let us consider 2×3 states. By making the propagated PMF sufficiently narrow at the multiple slit plane, so that $\xi_2 \approx 0$ in Eq. (6), the resulting state will be

$$|\psi_I\rangle \propto |-\tfrac{1}{2}\rangle(e^{i\varphi}E_2|-1\rangle + E_1|0\rangle) + |\tfrac{1}{2}\rangle(e^{i\varphi}E_2|1\rangle + E_1|0\rangle). \tag{8}$$

It is important to highlight that the number of possible states obtained by manipulating the PMF is limited for two reasons. First, since PMF shape is determined by the crystal properties, we can only modify the width of its image at z_a, Fig. 1, which implies an intrinsic limitation in the number of possible prepared two-qudit or qubit-qutrit states. If one wishes to make some $\xi_j = 0$, all the other terms $\xi_{j'}$ with $j' > j$ will be immediately canceled out. The second limitation can be observed from color code (shape code) in Eqs. (6) and (7): different pairs of modes are predominantly controlled by the same ξ_j. It is impossible to prepare a state with, for example, $|0\rangle|-3/2\rangle$ and without the $|-1\rangle|1/2\rangle$ term in Eq. (7), which is also a limitation in the type of prepared states related to the intrinsic spatial correlations of the photon pairs generated in SPDC [Eq. (5)].

B. Manipulating pump beam transverse profile

When a nonmagnified image of the plane at z_p is projected on z_a, the state of Eq. (4) can be written as

$$|\psi\rangle \propto \sum_{l_i=-\Lambda_i}^{\Lambda_i} \sum_{l_s=-\Lambda_s}^{\Lambda_s} e^{i\phi(l_i-l_s)^2} E\left(\frac{(l_i+l_s)d}{2}, z_p\right)|l_i\rangle|l_s\rangle, \tag{9}$$

where ϕ is a phase acquired along the propagation being dependent of the setup characteristics, and the biphoton is considered to propagate freely for a distance long enough to make the propagated PMF constant over all slits. For this case, we have the following coefficient matrix $M_{m\times n}$ for 2×3 and 3×4 dimensions, respectively:

$$M^{(\mathrm{pump})}_{2\times 3} = \begin{array}{c} \\ |-\frac{1}{2}\rangle \\ |\frac{1}{2}\rangle \end{array} \begin{array}{c} \begin{array}{ccc} |-1\rangle & |0\rangle & |1\rangle \end{array} \\ \begin{pmatrix} C_3 & C_1 & C_2 e^{2i\phi} \\ C_1 e^{2i\phi} & C_2 & C_4 \end{pmatrix} \end{array}, \tag{10}$$

and

$$M^{(\mathrm{pump})}_{3\times 4} = \begin{array}{c} \\ |-1\rangle \\ |0\rangle \\ |1\rangle \end{array} \begin{array}{c} \begin{array}{cccc} |-\frac{3}{2}\rangle & |-\frac{1}{2}\rangle & |\frac{1}{2}\rangle & |\frac{3}{2}\rangle \end{array} \\ \begin{pmatrix} C_5 & C_3 & C_1 e^{2i\phi} & C_2 e^{9i\phi/4} \\ C_3 e^{2i\phi} & C_1 & C_2 & C_4 e^{2i\phi} \\ C_1 e^{9i\phi/4} & C_2 e^{2i\phi} & C_4 & C_6 \end{pmatrix} \end{array}, \tag{11}$$

where $C_{1(2)} = E(-(+)\frac{d}{4}, z_p)$, $C_{3(4)} = E(-(+)\frac{3d}{4}, z_p)$, and $C_{5(6)} = E(-(+)\frac{5d}{4}, z_p)$.

In this situation we can "slice" the pump beam profile, at z_p, around the transverse positions indicated in Eqs. (10) and (11), instead of modifying only its image width. This increases the number of possible states that can be prepared but the limitation indicated by the color code (figures with same shape

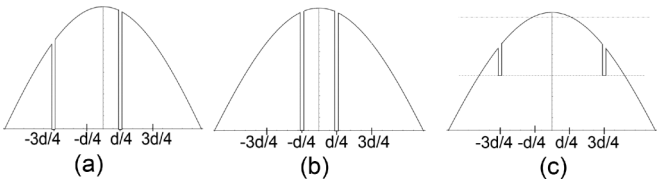

FIG. 2. Graphical representation of the profiles that produce the states $|\psi_{II}\rangle$, $|\psi_{III}\rangle$, and $|\psi_{IV}\rangle$.

and color tint) remains since different pairs of modes are controlled by the same C_j. This limitation comes from the linear momentum conservation in SPDC, which causes the same region of the pump beam transverse profile to control the correlations between more than one pair of slit modes. This feature remains even if different phases were added to different points of the pump profile, which shows that it is not a limitation associated with the manipulation method, but with the SPDC phenomenon itself.

Considering the dimension 2×3, we can take as an example states prepared by image projection (on z_a) of a pump beam profile with two dents as illustrated in Fig. 2. For instance, if we make these dents at $d/4$ and $-3d/4$, as shown in Fig. 1(a), we get the state

$$|\psi_{II}\rangle \propto \left|-\tfrac{1}{2}\right\rangle(C_3|-1\rangle + e^{2i\phi}C_2|1\rangle) + C_2\left|\tfrac{1}{2}\right\rangle|0\rangle, \quad (12)$$

which is nonmaximally entangled. If we make the dents in symmetrical regions with respect to the center of the arrangement, that is, in $\pm d/4$ as shown in Fig. 1(b), we get the state

$$|\psi_{III}\rangle \propto C_3\left|-\tfrac{1}{2}\right\rangle|-1\rangle + C_4\left|\tfrac{1}{2}\right\rangle|1\rangle, \quad (13)$$

which is maximally entangled if the pump profile is symmetrical, that is, if $C_3 = C_4$ before the manipulation, as in the case of an initial Gaussian beam.

The state $|\psi_{III}\rangle$ in Eq. (13), maximally or nonmaximally entangled, does not access all the base states, i.e., all the path states in the qutrit space. Because of that, $|\psi_{III}\rangle$ behavior is similar to a 2×2 state.

Moreover, this leads us to ask what shape of the pump beam would produce maximally entangled states in which all slits are accessed. For answering this question, we resort to the Schmidt decomposition [49]: given a bipartite pure state of dimension $m \times n$, and assuming $m \leqslant n$, a maximally entangled state in such decomposition would have all Schmidt coefficients equal to $1/\sqrt{m}$.

Schmidt coefficients can be obtained from the eigenvalues of the reduced density operator of the bipartite system. The non-null eigenvalues are equal to the square of the Schmidt coefficients. Considering a pure state, such as in Eq. (9), prepared with a symmetric pump beam transverse profile and considering $\Lambda_i = 2$ and $\Lambda_s = 3$, we have that the non-null eigenvalues of both qubit and qutrit will be equal to $1/\sqrt{2}$ if

$$C_3 = -\frac{C_1}{2\cos(2\phi)}, \quad (14)$$

with $C_4 = C_3$ and $C_2 = C_1$.

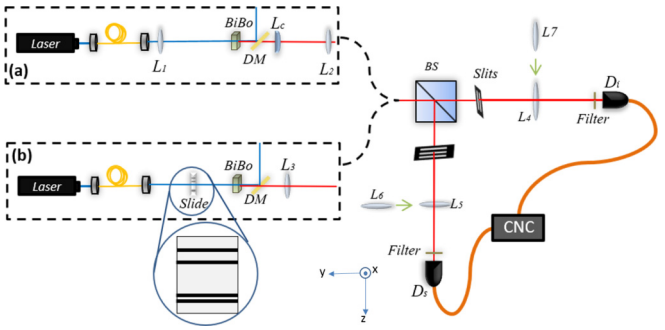

FIG. 3. Experimental setup for the preparation and detection of the 2×3 photonic spatial states. In (a) the magnified crystal image is projected on slits by a nonconfocal telescope. In (b), dark stripes have their images projected on the slits plane.

In the special case where $2\phi = \pi$ we get the state

$$|\psi_{IV}\rangle = \frac{1}{\sqrt{2}}\left\{\left|-\frac{1}{2}\right\rangle\left[\frac{3}{2}\left(-\frac{1}{2}|-1\rangle + |0\rangle + |1\rangle\right)\right] + \left|\frac{1}{2}\right\rangle\left[\frac{3}{2}\left(|-1\rangle + |0\rangle - \frac{1}{2}|1\rangle\right)\right]\right\}, \quad (15)$$

which can be rewritten in the form

$$|\psi_{IV}\rangle = \frac{1}{\sqrt{2}}\left\{\left|-\frac{1}{2}\right\rangle|\Omega_1\rangle + \left|\frac{1}{2}\right\rangle|\Omega_2\rangle\right\}, \quad (16)$$

where $|\Omega_1\rangle$ and $|\Omega_2\rangle$ are equal to

$$|\Omega_1\rangle = \tfrac{3}{2}\left(-\tfrac{1}{2}|-1\rangle + |0\rangle + |1\rangle\right),$$
$$|\Omega_2\rangle = \tfrac{3}{2}\left(|-1\rangle + |0\rangle - \tfrac{1}{2}|1\rangle\right). \quad (17)$$

The pump transverse profile with which one could prepare the state in Eq. (15) is shown in Fig. 1(c). The amplitude in $\pm 3d/4$ must be equal to half of the amplitude in $\pm d/4$. Besides that, the setup must be adjusted in order to make the propagation phase ϕ equal to $\pi/2$. The necessity of controlling the phase ϕ and the intensity along the profile, instead of just canceling it in some points, makes the preparation of this state more difficult.

IV. EXPERIMENT

Figure 3 shows our setup for preparation and measurement of 2×3 states, which could be used for any dimension. A 405 nm continuous-wave (cw) laser beam is filtered by a monomode fiber in order to ensure a stable pump beam. The preparation sequence is made in two ways. In Fig. 3(a), a 50 cm focal length lens (L_1) focuses the pump in the center of a BiB_3O_6 (BiBO) crystal, generating collinear 810 nm photon pairs in a type-I phase matching configuration. Next to the crystal, a 5 cm focal cylindrical lens (L_c) and a 20 cm spherical lens (L_2) form a nonconfocal telescope that projects the crystal image (z_0), with fourfold magnification, on the slits plane (z_a). In Fig. 3(b) the laser crosses a transparent slide with some printed black narrow lines, on the plane at z_p, before pumping the crystal. After that, a 12.5 cm spherical

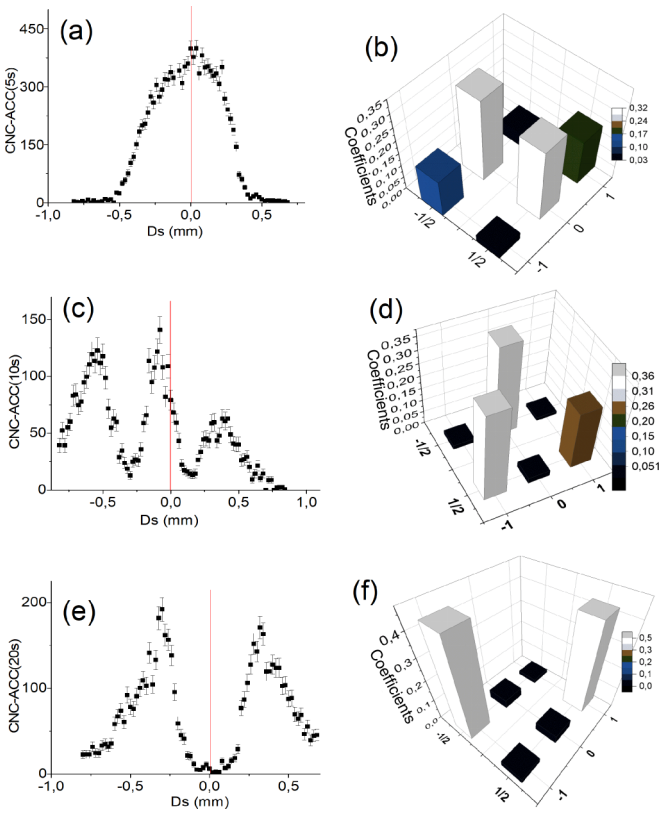

FIG. 4. Experimental pump beam profile at z_p and z_a planes, and the respective coefficients matrices for the states ψ_I [in (a) and (b)], ψ_{II} [in (c) and (d)], and ψ_{III} [in (e) and (f)]. The bars indicate the square of the absolute values of the coefficients in Eqs. (10) and (6). The red lines (the central lines) in (a), (c), and (e) indicate the region matched with the center of both multiple slits.

lens (L_3) projects, on the plane at z_a, a nonmagnified image of the plane at z_p.

In both configurations [Figs. 3(a) and 3(b)] a dichroic mirror (DM) reflects the pump beam out of the setup, and the twin photons are separated by a nonpolarized beam splitter (BS). Transmitted and reflected photons cross, respectively, double and triple slits which are positioned at the same distance from the BS. The slits are 100 μm wide and separated, center to center, by 250 μm. Furthermore, double and triple slits are positioned with their centers always coinciding with the center of the pump beam profile. The stripes shown in Fig. 3(b) are positioned so that they match with the transverse positions highlighted in Eq. (10). The single-photon detectors (D_i and D_s) are placed at a distance of 40 cm from the slits. Spherical lenses of 10 cm (L_4 and L_5) and 20 cm (L_6 and L_7) are used to perform, respectively, image and interference measurements. Interference filters, centered in 810 nm and 30 nm bandwidth, are coupled to detectors and microscope lenses are attached to the filters in order to couple the photons into multimode fibers. Rectangular apertures are placed at the entrances of the detectors (except for marginal measurements) in such a way that the scanning is made along the x direction. Coincidence counts are registered in a time window of 5 ns. Figures 4(a), 4(c), and 4(e) show different biphoton profiles on the z_a plane, obtained with both configurations shown in Fig. 3.

A. Correlation measurements in position-position basis

We characterize the states starting from measurements in position-position basis. For that, we use a lens to project the image of the two multiple slits in their respective detectors planes. We scan one of the detectors, while the other is maintained fixed in the center of each slit image. These measurements allow us determine experimentally the matrix coefficients [Eqs. (6) and (10)] for each of the prepared states, as shown in Figs. 4(b), 4(d), and 4(f).

Comparing Eq. (6) and the matrix in Fig. 4(b), we can conclude that the correlations are governed, predominantly, by the propagated phase matching; in other words, $\xi_1/\xi_2 \gg E_1/E_2$ as expected. We also observe that the experimental biphoton profile is not symmetrical, which produces the difference between $|-\frac{1}{2}\,-1\rangle$ and $|\frac{1}{2}1\rangle$ coefficients. For the second configuration in Fig. 3(b), a similar asymmetry between $|\frac{1}{2}\,-1\rangle$ and $|\frac{1}{2}1\rangle$ coefficients is theoretically expected and can be verified in the matrices in Figs. 4(d) and 4(f).

B. Qualitative characterization by measurements in position-momentum basis

A second measurement that we use to characterize the states qualitatively is projecting one of the multiple slits Fourier transforms over the respective detection plane. In this case we implement different measurement operators for each part of the state, that is, the measurements are made in different bases simultaneously.

Labeling the idler and signal photons as p or q, i.e., $p(q) = i, s(i, s)$, we will consider that the apertures plane of photon p is imaged at its detection plane, while the Fourier transform of the apertures plane of the photon q is projected at the second detection plane. In this case we can write the probability to get CNC as

$$P_2(x_i, x_s) \propto \mathrm{sinc}^2(\theta x_p)\left|\sum_{l_p}\sum_{l_q}\Phi_{\mathrm{in}}(l_p d, l_q d, z_a)e^{-i\gamma l_p x_p}\right.$$
$$\left.\times\prod\left(\frac{x_q - l_q d}{2a}\right)\right|^2, \tag{18}$$

where $\prod(x)$ is the rectangular function, which corresponds to the transmission function of a slit, and its presence in Eq. (18) is due to the image measurement. Owing to the rectangular function orthogonality (because the separation d is larger than the slits width $2a$), we can rewrite Eq. (18) as

$$P_2(x_p, x_q) \propto \mathrm{sinc}^2(\theta x_p)\sum_{l_p=-\Lambda_p}^{\Lambda_p}\sum_{l_q=-\Lambda_q}^{\Lambda_q}\prod\left(\frac{x_q - l_q d}{2a}\right)F_{\psi}^{(l_q)}(x_p). \tag{19}$$

This expression shows that different interference patterns can be observed when the detector of photon q is fixed in the center of each image slit. The oscillation described by $F_{\psi}^{(1)}(x_q)$ is governed by the global state coefficients $\Phi_{\mathrm{in}}(l_p d, l_q d, z_a)$ and also depends on which part of the system, as well as its dimension, is detected at the optical Fourier transform plane. Tables I and II show the expressions $F_{\psi}^{(l_q)}(x_p)$ for each 2×3 theoretical state presented above.

TABLE I. Theoretical oscillation functions when the qubit detector is kept fixed at the center of a slit image while the qutrit detector is scanned on the Fourier transform plane.

State	$F_{\psi}^{(-1)}(x_i)$	$F_{\psi}^{(0)}(x_i)$	$F_{\psi}^{(1)}(x_i)$
$\|\psi_I\rangle$	1	$[1-\cos(\gamma x_i)]$	1
$\|\psi_{II}\rangle$	1	1	1
$\|\psi_{III}\rangle$	1	0	1
$\|\psi_{IV}\rangle$	$[1-\frac{4}{5}\cos(\gamma x_i)]$	$[1-\cos(\gamma x_i)]$	$[1-\frac{4}{5}\cos(\gamma x_i)]$

The experimental interference patterns, measured in coincidences, for each state in Fig. 4 are shown in Fig. 5, where we can observe a more pronounced variance between theoretical curves of Tables I and II and the experimental data. The influence of the not null coefficients indicated by dark bars (the smaller bars) in Figs. 4(b), 4(d) and 4(f) can be clearly seen in the patterns obtained from qubit far-field measurements. Despite this, we can see a strong agreement between the experimental patterns and the expected curves for the real coefficients' values, which are shown in lines superimposed to the experimental dots in Fig. 5. We are not yet able to link a global state feature to the oscillations $F_{\psi}^{(l_q)}(x_p)$ directly but they seem, together, to give us a state signature.

C. Qualitative characterization by marginal measurements

We explore a third kind of measurement where one of the detectors is maintained open while the other is scanned in the Fourier transform plane; in other words, we measure marginal probabilities in the momentum basis. Labeling the photons as in the previous subsection, the probability to detect the twin photons in coincidences, as functions of the detector position of the photon q and using the photon p as a trigger, i.e., a heralded single photon detection, is

$$P_1(x_q) \propto \mathrm{sinc}^2(\theta x_q) \sum_{l_p} \sum_{l_q} \sum_{l'_q} \Phi_{\mathrm{in}}(l_p d, l_q d, z_a) \times \Phi^*_{\mathrm{in}}(l_p d, l'_q d, z_a) e^{i\gamma (l'_q - l_q) x_q}, \quad (20)$$

which we can write in the simple form

$$P_1(x_q) \propto \mathrm{sinc}^2(\theta x_q) F_{\psi}^{(1)}(x_q), \quad (21)$$

where $F_{\psi}^{(1)}(x_q)$ is a marginal oscillation function.

For pure Bell states, it was already shown that the amount of entanglement is directly linked to marginal pattern contrast. Bipartite states in which the marginal interference pattern presents a minimal visibility have maximal concurrence [15]. Furthermore, some $m \times m$ maximally entangled states (that anticorrelated one) have diagonal reduced density operators which do not provide fringes in marginal measurement. Therefore, the absence of interference fringes in these cases is an indication of maximal entanglement, but the same is not valid for the states presented in this work.

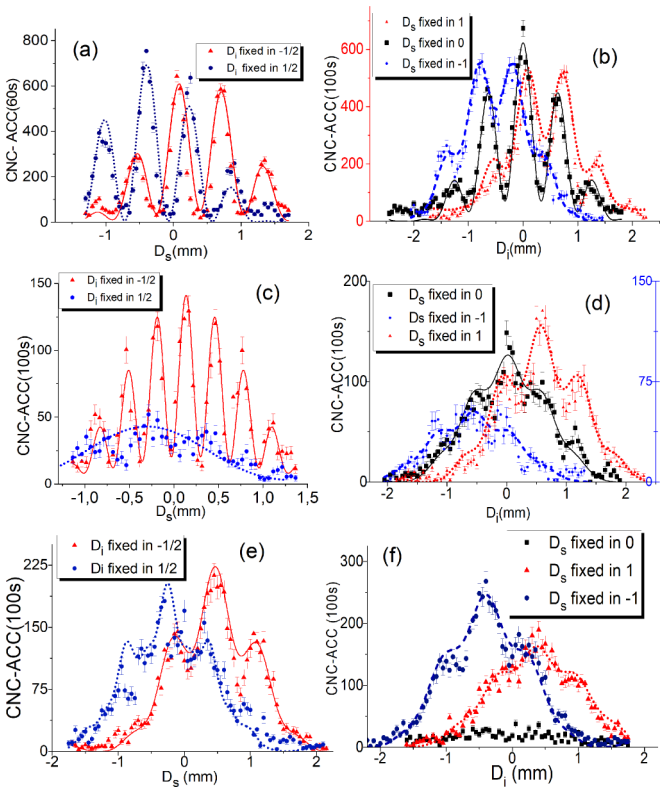

FIG. 5. Interference patterns measured in hybrid detection. In (a), (c), and (e) D_i was fixed in peaks regarding the down and up apertures of double slit; in (b), (d), and (f) D_s was fixed in peaks regarding the down, up, and middle apertures of triple slit. The dots (circles, squares, and triangles) are the experimental data with error bars and the lines (solid, dash, and dot dash lines) are the expected curves drescribed in Eq. (18) for the states with the coefficients shown in the matrices in Fig. 4. The interference patterns in (a) and (b) correspond to the coefficients in Fig. 4(b), (c) and (d) correspond to the coefficients in Fig. 4(d), and (e) and (f) correspond to the coefficients in Fig. 4(f).

It is important to observe that, in general, each part of an $m \times n$ state ($m < n$) provides different marginal interference patterns due to the dimension asymmetry. Therefore, we must take into account which part is chosen when we analyze the global state by averaging one part of it. The results of

TABLE II. Theoretical oscillation functions when the qutrit detector is kept fixed at the center of a slit image while the qubit detector is scanned on the Fourier transform plane.

State	$F_{\psi}^{(-1/2)}(x_s)$	$F_{\psi}^{(1/2)}(x_s)$
$\|\psi_I\rangle$	$[1+\cos(\gamma x_s)]$	$[1+\cos(\gamma x_s)]$
$\|\psi_{II}\rangle$	1	$[1+\frac{2C_3C_2}{C_3^2+C_2^2}\cos(\phi d^2)\cos(2\gamma x_s)]$
$\|\psi_{III}\rangle$	1	1
$\|\psi_{IV}\rangle$	$[1+\frac{4}{9}(\cos(\gamma x_s)-\cos(2\gamma x_s))]$	$[1+\frac{4}{9}(\cos(\gamma x_s)-\cos(2\gamma x_s))]$

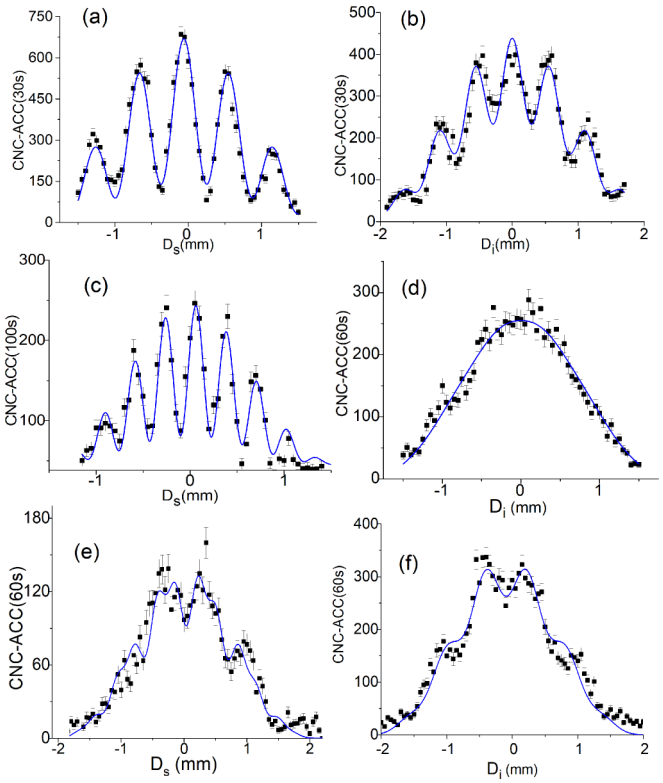

FIG. 6. Interference patterns measured in marginal detection. In (a), (c), and (e) D_i is open and in (b), (d), and (f) D_s is open. The dots are the experimental data with error bar and the blue (solid) lines are the expected theoretical curves described in Eq. (20) for the states with the real coefficient values of Figs. 4(b), 4(d), and 4(f). The interference patterns in (a) and (b) correspond to the coefficients in Fig. 4(b), (c) and (d) correspond to the coefficients in Fig. 4(d), and (e) and (f) correspond to the coefficients in Fig. 4(f).

both marginal measurements may even be different, but they must lead to the same, or nonconflicting, conclusion about the global state properties. This reinforces the requirement to study marginal probabilities considering the different properties of the dimensions composing a higher dimensions system.

Among the states introduced previously, $|\psi_{III}\rangle$ is a maximally entangled one that exhibits the same behavior as a Bell state, so both marginal probabilities do not present oscillations. The state $|\psi_{IV}\rangle$ has maximal concurrence but, however, has the qutrit part exhibiting interference on the marginal probability, even the state having maximal concurrence. For $|\psi_{IV}\rangle$,

$$F^{(1)}_{\psi_{IV}}(x_i) = 1,$$
$$F^{(1)}_{\psi_{IV}}(x_s) = 1 + \tfrac{4}{9}[\cos(\gamma x_s) - \cos(\gamma 2x_s)]. \quad (22)$$

On the other hand, the state $|\psi_{II}\rangle$, despite being nonmaximally entangled, has no oscillations on marginal probability when it is measured by scanning the detector of the qubit part, namely

$$F^{(1)}_{\psi_{II}}(x_i) = 1,$$
$$F^{(1)}_{\psi_{II}}(x_s) = 1 + \frac{2C_3C_2}{2C_2^2 + C_3^2}\cos(2\phi d^2 - 2\gamma x_s). \quad (23)$$

Finally, the state $|\psi_I\rangle$ is also nonmaximally entangled and its both parts exhibit oscillations as expected in principle:

$$F^{(1)}_{\psi_I}(x_i) = 1 + \tfrac{1}{2}\cos(\gamma x_i),$$
$$F^{(1)}_{\psi_I}(x_s) = 1 + \cos(\gamma x_i + \varphi) + \cos(\gamma x_i - \varphi). \quad (24)$$

Experimental marginal patterns for the states shown in Fig. 4 are presented in Fig. 6. Again, the experimental data is in agreement with the expected curves for states with the coefficients shown in Figs. 4(b), 4(d), and 4(f).

V. OBSERVATION CONCERNING CONDITIONAL TERMS IN MEASUREMENTS IN MOMENTUM-MOMENTUM BASIS

If we use a lens to project the Fourier transform of both multiple slits in the detection planes, the probability to get coincidence as a function of the detectors' position along x direction is

$$P_2(x_i, x_s) \propto \mathrm{sinc}^2(\theta x_s)\mathrm{sinc}^2(\theta x_i)F^{(2)}_{\psi}(x_i, x_s), \quad (25)$$

where $\theta \equiv ka/(2f)$, a is the separation between two apertures, f is the focal distance of the lens, and $F^{(2)}_{\psi}(x_i, x_s)$ is a function that describes the spatial oscillation weighted by the state coefficients $\Phi_{\mathrm{in}}(l_i d, l_s d, z_a)$.

For maximally entangled states like Bell states, in 2×2 dimension, and anticorrelated in $m \times m$ dimension, $F^{(2)}_{\psi}(x_i, x_s)$ has only oscillatory terms dependent on $x_i \pm x_s$, identified as conditional terms. Because of that, it is usual to associate maximal entanglement with the presence of this kind of oscillation only. However, in most of the $m \times n$ states ($m \neq n$) one mode from the first part is correlated with a superposition of modes from the second part and because of that we cannot link directly entanglement and conditional oscillations. The state of Eq. (15), for example, has an oscillation function

$$F_{\psi_{IV}}(x_i, x_s) = \{1 + \tfrac{8}{9}\cos[\gamma(x_i - x_s)] - \tfrac{2}{9}\cos[\gamma(x_i - 2x_s)] - \tfrac{4}{9}\cos[\gamma(x_i + x_s)] - \tfrac{1}{9}\cos[\gamma(x_i + 2x_s)] - \tfrac{1}{9}\cos(\gamma x_i)\}, \quad (26)$$

which has a nonconditional term even though the entanglement formation of the state, as well its concurrence, is equal to one.

VI. DISCUSSION AND OUTLOOK

In this work, we studied the preparation of bipartite spatial quantum states with the parts having different dimensions which are determined by the number of multiple-slit ways set in the path of photons produced in the SPDC process. We presented experimentally the results of two-photons 2×3 states with some particular spatial correlations. We discussed the versatility and limitations in preparing the $m \times n$ quantum photonic states encoded in the photon paths degree of freedom, a consequence of transverse linear momentum conservation in SPDC.

We showed, mathematically and experimentally, the unusual behavior that these states can exhibit on far-field measurements and found agreement between the theoretical predicted interference patterns and the measured ones. We also pointed out that some behavior on far-field measurements requires more accurate analyses concerning, for example, the relation between marginal probabilities and entanglement measures, which will be explored in a future work. Finally, we introduce hybrid measurements which we show to be useful for spatial states' characterization and experiments concerning interferometric features. Our analyses open the range for possible applications using $m \times n$ quantum states, which are indispensable for experimental realizations of several theoretical works.

ACKNOWLEDGMENTS

This research was supported by the Brazilian agencies CNPQ - Conselho Nacional de Desenvolvimento Científico e Tecnológico, Capes - Coordenação de Aperfeiçoamento de Pessoal de Nível Superior, Fapemig - Fundação de Amparo á Pesquisa do Estado de Minas Gerais, and INCT-IQ - Instituto Nacional de Ciência e Tecnologia de Informação Quântica.

[1] T. Jennewein, C. Simon, G. Weihs, H. Weinfurter, and A. Zeilinger, Phys. Rev. Lett. **84**, 4729 (2000).
[2] D. Bouwmeester, J. W. Pan, K. Mattle, M. Eibl, H. Weinfurter, and A. Zeilinger, Nature (London) **390**, 575 (1997).
[3] B. Marques, M. R. Barros, W. M. Pimenta, M. A. D. Carvalho, J. Ferraz, R. C. Drumond, M. Terra Cunha, and S. Pádua, Phys. Rev. A **86**, 032306 (2012).
[4] C. K. Law and J. H. Eberly, Phys. Rev. Lett. **92**, 127903 (2004).
[5] C. H. Monken, P. H. Souto Ribeiro, and S. Paádua, Phys. Rev. A **57**, 3123 (1998).
[6] R. Ramírez-Alarcón, H. Cruz-Ramírez, and A. B. U'Ren, Laser Phys. **23**, 055204 (2013).
[7] W. P. Grice, A. B. U'Ren, and I. A. Walmsley, Phys. Rev. A **64**, 063815 (2001).
[8] M. V. Fedorov, M. A. Efremov, P. A. Volkov, E. V. Moreva, S. S. Straupe, and S. P. Kulik, Phys. Rev. Lett. **99**, 063901 (2007).
[9] A. G. da Costa Moura, W. A. T. Nogueira, and C. H. Monken, Opt. Commun. **283**, 2866 (2010).
[10] W. H. Peeters, J. J. Renema, and M. P. van Exter, Phys. Rev. A **79**, 043817 (2009).
[11] M. V. Jabir, N. A. Chaitanya, and G. K. Samanta, Front. Opt. paper JTh2A. **18** (2016).
[12] H. J. Lee and H. S. Park, Quantum Inf. M. paper QF2B. **2** (2017).
[13] D. Ghosh, T. Jennewein, P. Kolenderski, and U. Sinha, OSA Cont. **1**, 996 (2018).
[14] E. J. S. Fonseca, J. C. Machado da Silva, C. H. Monken, and S. Pádua, Phys. Rev. A **61**, 023801 (2000).
[15] L. Neves, G. Lima, E. J. S. Fonseca, L. Davidovich, and S. Pádua, Phys. Rev. A **76**, 032314 (2007).
[16] E. V. Kovlakov, S. S. Straupe, and S. P. Kulik, Phys. Rev. A **98**, 060301(R) (2018).
[17] S. Liu, Z. Zhou, S. Liu, Y. Li, Y. Li, C. Yang, Z. Xu, Z. Liu, G. Guo, and B. Shi, Phys. Rev. A **98**, 062316 (2018).
[18] C. J. Pugh, P. Kolenderski, C. Scarcella, A. Tosi, and T. Jennewein, Opt. Express **24**, 20947 (2016).
[19] H. Avetisyan and C. H. Monken, Opt. Express **24**, 2318 (2016).
[20] R. Shimizu, T. Yamaguchi, Y. Mitsumori, H. Kosaka, and K. Edamatsu, Phys. Rev. A **77**, 032338 (2008).
[21] A. Mair, A. Vaziri, and G. A. Zeilinger, Nature (London) **412**, 313 (2001).
[22] W. H. Peeters, E. J. K. Verstegen, and M. P. van Exter, Phys. Rev. A **76**, 042302 (2007).
[23] A. K. Jha, B. Jack, E. Yao, J. Leach, R. W. Boyd, G. S. Buller, S. M. Barnett, S. Franke-Arnold, and M. J. Padgett, Phys. Rev. A **78**, 043810 (2008).
[24] D. Pagel and H. Fehske, J. Phys. B: At. Mol. Opt. Phys. **50**, 224002 (2017).
[25] L. Neves, G. Lima, J. G. Aguirre Gómez, C. H. Monken, C. Saavedra, and S. Pádua, Phys. Rev. Lett. **94**, 100501 (2005).
[26] G. Lima, L. Neves, I. F. Santos, C. H. Monken, J. G. A. Gómez, C. Saavedra, and S. Pádua, Int. J. Quantum Inf. **05**, 69 (2007).
[27] B. P. Lanyon, T. J. Weinhold, N. K. Langford, J. L. O'Brien, K. J. Resch, A. Gilchrist, and A. G. White, Phys. Rev. Lett. **100**, 060504 (2008).
[28] L. Neves, G. Lima, A. Delgado, and C. Saavedra, Phys. Rev. A **80**, 042322 (2009).
[29] A. Z. Khoury and L. E. Oxman, Phys. Rev. A **89**, 032106 (2014).
[30] K. Ann and G. Jaeger, Phys. Lett. A **372**, 579 (2008).
[31] G. Karpat and Z. Gedik, Phys. Lett. A **375**, 4166 (2011).
[32] H.-R. Wei, B.-C. Ren, and F.-G. Deng, Quantum Inf. Process. **12**, 1109 (2013).
[33] D. Girolami, T. Tufarelli, and G. Adesso, Phys. Rev. Lett. **110**, 240402 (2013).
[34] H. Zhao, S.-M. Fei, J. Fan, and Z.-X. Wang, Int. J. Quantum Inf. **12**, 1450013 (2014).
[35] X. Zhan, X. Zhang, J. Li, Y. Zhang, B. C. Sanders, and P. Xue, Phys. Rev. Lett. **116**, 090401 (2016).
[36] K. K. Sharma and S. N. Pandey, Quantum Inf. Process. **13**, 2017 (2014).
[37] Z.-G. Li, S.-M. Fei, Z. D. Wang, and W. M. Liu, Phys. Rev. A **79**, 024303 (2009).
[38] P. Faist, Ph.D. thesis, ETH Zurich, 2016.
[39] S. P. Walborn, C. H. Monken, S. Pádua, and P. H. Souto Ribeiro, Phys. Rep. **495**, 87 (2010).
[40] C. K. Hong and L. Mandel, Phys. Rev. A **31**, 2409 (1985).
[41] K. W. Chan, J. P. Torres, and J. H. Eberly, Phys. Rev. A **75**, 050101(R) (2007).
[42] S. S. Straupe, D. P. Ivanov, A. A. Kalinkin, I. B. Bobrov, and S. P. Kulik, Phys. Rev. A **83**, 060302(R) (2011).
[43] S. P. Walborn, D. S. Ether, R. L. de Matos Filho, and N. Zagury, Phys. Rev. A **76**, 033801 (2007).

[44] D. S. Tasca, S. P. Walborn, P. H. Souto Ribeiro, and F. Toscano, Phys. Rev. A **78**, 010304(R) (2008).
[45] D. S. Tasca, S. P. Walborn, P. H. Souto Ribeiro, F. Toscano, and P. Pellat-Finet, Phys. Rev. A **79**, 033801 (2009).
[46] L. Zhang, L. Neves, J. S. Lundeen, and I. A. Walmsley, J. Phys. B **42**, 114011 (2009).
[47] E. S. Gómez, W. A. T. Nogueira, C. H. Monken, and G. Lima, Opt. Exp. **20**, 3753 (2012).
[48] L. Neves, S. Pádua, and C. Saavedra, Phys. Rev. A **69**, 042305 (2004).
[49] C. Eltschka and J. Siewert, J. Phys. A: Math. Theor. **47**, 424005 (2014).